Observation of Anderson localization beyond the spectrum of the disorder

Alex Dikopoltsev
Technion

Sebastian Weidermann
UNiversity of Rostock

Mark Kremer
University of Rostock   https://orcid.org/0000-0003-2597-7259

Andrea Steinfurth
UNiversity of Rostock

Hanan Herzig Sheinfux
Institute of Photonic Sciences

Alexander Szameit
University of Rostock   https://orcid.org/0000-0003-0071-6941

Mordechai (Moti) Segev (✉ msegev@technion.ac.il)
Technion

Article

Observation of Anderson localization
beyond the spectrum of the disorder

Alex Dikopoltsev[1*], Sebastian Weidemann[2*], Mark Kremer[2*], Andrea Steinfurth[2],

Hanan Herzig Sheinfux[1,3], Alexander Szameit[2], and Mordechai Segev[1]

[1]Physics Department, Technion, 32000 Haifa, Israel
[2]Institute for Physics, University of Rostock, 18059 Rostock, Germany
[3]ICFO- Institute of Photonic Sciences, Mediterranean Technology Park, 08860 Castelldefels (Barcelona), Spain
*The authors contributed equally to this work

Anderson localization is a fundamental wave phenomenon predicting that transport in a 1D uncorrelated disordered system comes to a complete halt, experiencing no transport whatsoever. However, in reality, a disordered physical system is always correlated, because it must have a finite spectrum. Common wisdom in the field states that localization is dominant only for wavepackets whose spectral extent resides within the region of the wavenumber span of the disorder. Here, we experimentally observe that Anderson localization can occur and even be dominant for wavepackets residing entirely outside the spectral extent of the disorder. We study the evolution of waves in synthetic photonic lattices containing bandwidth-limited (correlated) disorder, and observe Anderson localization for wavepackets of high wavenumbers centered around twice the mean wavenumber of the disorder spectrum. Likewise, we predict and observe Anderson localization at low wavenumbers, also outside the spectral extent of the disorder, and find that localization there can be as strong as for first-order transitions. This feature is universal, common to all Hermitian wave systems, implying that low-wavenumber wavepackets localize with a short localization length even when the disorder is strictly at high wavenumbers. This understanding suggests that disordered media should be opaque for long-wavelengths even when the disorder is strictly at much shorter length scales. Our results shed light on fundamental aspects of physical disordered systems and offer avenues for employing spectrally-shaped disorder for controlling transport in systems containing disorder.

It has been known for two millennia that particles experience stochastic motion while falling through voids[1], which was later understood as random walk and diffusive motion. After the discovery of the electron, Paul Drude has shown[2] that indeed random walk is at the heart of electrical conduction, giving rise to Ohm's law. It came as a surprise, when half a century later, P.W. Anderson has argued that the wave nature of electrons plays a crucial role in their dynamics in random media, and predicted that interference effects can bring all transport to a complete halt[3]. This phenomenon of Anderson localization requires the potential to be stationary and the absence of interactions. However, electrons inevitably interact with one another; hence Anderson localization of electrons in solids remained elusive. However, almost four decades ago, it was realized that localization is a universal wave phenomenon[4–7], and since then was demonstrated in a variety of systems, ranging from light scattering in dielectric media[8–10], microwaves[11,12], and disordered photonic lattices[13–15], to sound waves[16] and cold atoms[17,18]. The study of waves in disordered media and localization is an extremely rich field, generating surprising novel phenomena such as Levy-flight [19], hyper-transport [20], localization by deep subwavelength disorder[21], and localization phenomena in unusual settings such as amorphous media [22,23], Moire lattices[24] and non-Hermitian systems[25].

The propagation of waves in random media is characterized by localized eigenstates with exponentially decaying tails, such that their ensemble average, taken over multiple realizations of the disorder, yields a measure called the localization length, l_{loc}, equal to the inverse of the decay rate. Using a universal model, it was predicted that in infinite 1D or 2D disordered systems, all eigenstates become exponentially localized[26]. The outcome is different for finite systems, where some eigenstates have l_{loc} larger than the system size L. These modes can facilitate transport in finite systems and are typically termed extended[27,28], whereas the modes with l_{loc} significantly

smaller than *L* are considered localized and do not support transport. However, transport in disordered systems also depends on the spectrum of the disorder. A physical system always has a characteristic length scale associated with the smallest size in the system (e.g., atoms); hence the spectrum of the disorder always has a finite extent. This implies that any disorder in physical systems is always correlated in space (through simple Fourier relations). The spectral extent of the disorder sets a bound on l_{loc} , which directly depends on the spatial correlations of the disorder[6,29–32]. It is therefore instructive to consider localization from a spectral perspective.

Consider a one-dimensional system with a disordered potential V(x). The spatial power spectrum of the disorder $S(k) \propto |FT\{V(x)\}|^2$, is the Fourier transform (FT) of the two-point correlation function of the potential, $C_v(x, x')$, and it determines the range of possible scattering processes allowed by the momentum exchanges between the waves and the disordered potential[27,29,32] (Fig. 1a). One may think of the localization phenomenon as the outcome of multiple scattering processes of waves from the disordered potential, where the disorder is constructed as an ensemble of random gratings whose wavenumbers define S(k). Every spectral component of the disorder behaves as a diffraction grating that scatters one plane wave component into another. The primary scattering process of a plane wave is mediated by only a single spectral component of the disorder, similar to a Bragg reflection off a grating with a spectral component k. Having many transitions of such first-order scattering events from a collection of gratings with random amplitudes and phases (constituting the disordered system) is eventually manifested in the Anderson localization phenomenon.

Accordingly, for localization mediated by first-order transitions, the localization length l_{loc} is inversely proportional to the mean amplitude of the power spectrum of the disorder, $S(k)$[33]. Following this reasoning, it seemed for some time that localization in systems with correlated

disorder can occur only for wavepackets whose spectrum is fully contained within the spectral extent of the disorder[12,17,27,34]. However, it was later found that localization can also be induced by two (or more) consecutive contributions of the potential[33,35,36], which may lead to localization outside the spectral extent of S(k). We henceforth refer to the scattering processes involving intermediate wavenumbers outside the spectrum of the disorder as "virtual", in analogy (explained later) to atomic transitions through virtual energy level. Generally, such second-order processes are significantly weaker than first-order transitions. Consequently, thus far - in all experiments showing Anderson localization in all fields of science, the contribution came from 'first-order' transitions. Therefore - experimentally - Anderson localization was always limited to the spectral reach of the disorder[8,10–14,16–18].

Here, we observe Anderson localization for wavepackets residing entirely outside the spectral extent of the disorder, mitigated solely by virtual transitions. Our experiments are carried out in synthetic photonic lattices containing bandwidth-limited disorder, and demonstrate how virtual (two-step) transitions lead to Anderson localization around twice the mean wavenumber of the disorder. In addition, we predict and observe universal localization at low wavenumbers, implying that any low-wavenumber wave packet can strongly, localize even when the disorder is strictly at high wavenumbers. The underlying mechanism requires only for the spectrum of the disorder to be symmetric, irrespective of its spectral shape. The symmetric transitions, which are natural to any Hermitian system, induce scattering to virtual states and back, and eventually lead to very short localization lengths for low-wavenumber wavepackets.

We begin by explaining the underlying concepts using the transverse localization scheme[7,13] as a convenient example to frame the discussion. This scheme exploits the mathematical equivalence between the paraxial wave equation for light and the Schrödinger equation (see first section of the

SI[37]). This equivalence has been used to experimentally observe a plethora of wave phenomena for the first time, such as, for example, Floquet topological insulators[38], bound states in the continuum[39], topological Anderson insulators[40] and Anderson localization in a lattice containing disorder[13]. The paraxial wave equation for the slowly-varying amplitude of the light propagating in a 2D dielectric medium is

$$i\frac{\partial \psi(x,z)}{\partial z} = -\frac{1}{2\beta_0}\frac{\partial^2}{\partial x^2}\psi(x,z) - \frac{\beta_0}{n_0}\Delta n(x)\psi(x,z) \quad (1),$$

where $\beta_0 = \omega n_0/c$ is the wavenumber, z is the propagation direction (analogous to time in the Schrödinger equation), n_0 is the ambient refractive index and $\Delta n(\text{x})$ is spatially-varying perturbation on n_0 the acts as a random and stationary potential. In this system, wavefunctions $\psi(\text{x},\text{z})$ with wavenumbers within the spectral extent of the disorder, can become localized after some finite propagation distance[7,13,14,41]. From the linearity of the equations, $\Delta n(\text{x})$ can be written as a superposition of periodic functions, each acting as a grating component causing the spectral components of $\psi(\text{x},\text{z})$ to experience diffraction off this grating (Fig. 1a)[1]. Hence, localization may be viewed as an ensemble of waves diffracting from a random superposition of gratings, each with its spatial wavenumber[42]. Therefore, it is instructive to examine a disordered system in momentum space. The evolution of a wave packet in k-space is defined by the spatial FT of Eq. (1)

$$i\frac{\partial \tilde{\psi}(k,z)}{\partial z} = \frac{1}{2\beta_0}k^2\tilde{\psi}(k,z) - \frac{\beta_0}{n_0}\int \Delta \tilde{n}(k')\tilde{\psi}(k-k')dk' \quad (2),$$

where $\tilde{\psi}(\text{k},\text{z})$ and $\Delta \tilde{n}(\text{k})$ are the FT of $\psi(\text{x},\text{z})$ and $\Delta n(\text{x})$, respectively. In the RHS of (2), we can treat plane waves as eigenstates of a spatially homogeneous system, with the disorder coupling between them by convolutions with components in the spectrum of the disorder. These transitions

---

[1] The sketch in Fig. 1a illustrates reflection from a random superposition of gratings. In reality, Eq. 1 describes EM waves in the paraxial regime, hence the reflections are all at shallow angles.

in momentum space are naturally described by coupled-mode formalism. The coupling between two different plane waves can occur if the potential contains a suitable disorder component that can momentum-match between the incident and scattered waves (Fig. 1a). Employing this coupled-mode formalism is fully equivalent to solving Eq. (1) in real space, and it is regularly used in analyzing wave phenomena. It relies on phase-matched interactions, which, in the analogous Schrödinger equation represent transitions that conserve energy.

Consider first a disordered potential $\Delta n(x)$ such that its spectrum $\Delta \tilde{n}(k)$ consists of two regions in momentum-space, with random amplitude and phase (Fig. 1b). Let us assume that spectral regions of the disorder are nonzero only in a small region Δk around wavenumbers $\pm k_0$. When $\Delta n(x)$ is real (as in our optical experiments, where photonic system is Hermitian), $|\Delta \tilde{n}(k)|$ is symmetric. For a plane wave incident upon this potential with wavenumber $k_{in} \approx -k_0/2$, there are many possible phase-matched first-order transitions to the spectral region around $k_0/2$, obeying the paraxial dispersion relation $\beta(k_{in}) = \beta(k_0/2)$, where $\beta(k) = \beta_0 - k^2/2\beta_0$ (see first section of the SI[37]). This plane wave undergoes many sequential first-order transitions, from positive to negative wavenumbers and back, leading to the buildup of Anderson localization[42]. In this process, the spectrum of the localized wave packet reshapes but remains confined around $\pm k_0/2$.

However, our primary interest here are plane-waves for which no phase-matched first-order transitions exist, and, hence, only second-order ones can contribute to localization. For an incident wave with wavenumber $k_{in} \approx -k_0$, the first-order transitions in the bandwidth-limited potential of Fig. 1b, namely, $-k_0 \xrightarrow{-k_0} -2k_0$ and $-k_0 \xrightarrow{+k_0} 0$, are not phase-matched. Yet, the two-step transition $-k_0 \xrightarrow{+k_0} 0 \xrightarrow{+k_0} k_0$, is in fact phase-matched. We call the sequential transition "virtual"

because energy does not accumulate in the intermediate state at $k = 0$, in similarity to the role played by virtual levels in atomic systems (Fig. 1c). This transition requires two scattering events mediated by two spectral components (two random gratings), which may have the same or different wavenumbers, as long as both gratings have nonzero amplitudes, i.e., they are both contained within the spectral extent of the correlated disorder[36].

To study the process of localization driven by spectrally-shaped disorder, we investigate the evolution of wave packets with different initial wavenumbers $k_{in} \in \{0, 1.25k_0\}$ in our system with bandwidth-limited disorder centered around k_0 with width $0.25k_0$ (Fig. 2).). The creation of the bandwidth-limited disorder is explained in the second section of the SI[37]. To describe the physics of random processes, statistical tools are required and hence, meaningful results are obtained from ensemble-averaging over multiple realizations of the disorder[13,41] (see third section in the SI[37]). Figure 2a shows the propagation of the ensemble-averaged wave packets in the bandwidth-limited disorder. At $k_{in} = 0$, the wavepacket evolves without expanding, due to second-order processes. In the absence of disorder (i.e., in a homogeneous medium), the same input wavepacket expands by ~5 times, for the same propagation distance. Thus, the absence of diffraction-broadening due to disorder is a clear and direct evidence for localization by two-step processes. At $k_{in} = 0.25k_0$ the wavepacket is within the spectral extent of the strong disorder, hence the localizes by bandwidth increase (see discussion in the fourth section of the SI[37]). For $k_{in} = k_0/2$, multiple first-order transitions are phase-matched, hence the wavepacket is localized: its expansion stops and it propagates on-axis despite its initial momentum. This case is the ordinary outcome of Anderson localization. On the other hand, for $k_{in} = 0.83k_0$ the transitions are phase-mismatched, so the wavepacket expands as if it is unaffected by the disorder, and propagates at its initial trajectory. When $k_{in} = k_0$, we again find evolution in the regime of second-order localization.

Initially, the wavepacket expands, but after some distance the expansion stops and the propagation is on-axis. The lack of expansion and the on-axis propagation prove that this case is again localization by two-step processes. For $k_{in} = 1.25k_0$,the transitions are again phase-mismatched, so the wavepacket is (again) unaffected by the disorder: it expands and continues on its initial trajectory.

The most important signature of a wavepacket that underwent localization is the asymptotic stop of its expansion. To quantify the width of the wavepackets and compare the expansion for different angles, we use the effective width[13], w_{eff}, which is the width of the ensemble-averaged wavefunction of the intensity, with the ensemble taken over many realizations of the disorder of the same characteristics (power spectrum, average amplitude, etc.)[13]. For a 1D exponentially-decaying function, w_{eff} is equal to localization length l_{loc}. Figure 2b shows the effective width w_{eff} for several initial momenta. We mark the regions where w_{eff} is reduced by the scattering process (indicative for localization) and divide them into two types: (i) a region driven by first-order transitions (orange), where we find a local minimum around $k_{in} = k_0/2$, and (ii) regions where only second-order processes dominate, where we find local minima in w_{eff} at $k_{in} = 0$ and k_0. The low effective width at $k_{in} = k_0$ is a direct result of strictly second-order localization processes. The very low w_{eff} at low wavenumbers ($k_{in} \sim 0$) implies that – even though second-order processes are generally weak – wavepackets with low group velocities can localize, with localization as strong as first-order localization. These simulations prove that wavepackets with wavenumber k_0, which are outside of the immediate influence zone of the potential, indeed become localized. Altogether, as shown in Fig. 2, these multiple scattering processes induce Anderson localization by virtual transitions, with the localized wavepackets residing completely

outside the spectral extent of the disorder, specifically - at twice the first-order localization wavenumbers, and also at very low wavenumbers at the vicinity of zero.

To experimentally demonstrate Anderson localization strictly by second-order scattering, we employ a synthetic one-dimensional photonic lattice encoded in a time-bin system based on the propagation of light in coupled optical fiber loops[43–45]. The implementation is based on the idea, that the dynamics in a 1+1 dimensional double-discrete lattice (Fig. 3a), which is similar to the quantum walk of a single particle, describes the propagation of light pulses in the coupled fiber loops (Fig. 3c). The corresponding mapping between the propagation of light and the evolution in the synthetic lattice is explained in fifth section of the SI[37]. The precisely tunable optical system allows to create a multitude of photonic lattices, especially lattices with correlated disorder. This experimental setting allows to measure the squared modulus of the wavefunction at all steps of the evolution, such that one can obtain the full dynamics. Such fiber-loop photonic lattices have proven to be powerful for experimenting with numerous phenomena, such as Bloch oscillations and solitons in PT-symmetric systems[45–48], topological lattices[49], and even topological funneling of light[50].

The recursive equations describing the dynamics in our synthetic lattice are

$$
\begin{aligned}
u_n^{m+1} &= \tfrac{1}{\sqrt{2}}(u_{n+1}^m + iv_{n+1}^m)e^{i\varphi_u(n,m)} \\
v_n^{m+1} &= \tfrac{1}{\sqrt{2}}(iu_{n-1}^m + v_{n-1}^m)
\end{aligned}
\tag{3},
$$

where u_n^m, v_n^m are the complex amplitudes of the pulses, corresponding to the wavefunction, at lattice site position (time-bin) n and time step m, in the short and long fiber loops, respectively (Fig. 3b). The parameters of this time-bins system can be designed adjusted to correspond to the localization phenomena described by Eq. 1. Specifically in our system, we construct the real propagation-invariant potential, $\Delta n(x)$, by introducing phase modulation $\varphi_u = \varphi_u(n,m)$ in the u-

loop[44]. Hence, through the phase modulation φ_u we shape the disorder at will, and control its spectral properties. To evaluate the ensemble average characteristics, it is sufficient to consider the intensity distribution in one of the optical fibre loops. The reason for this is that the differences in the intensity distributions between the short and the long loop are only on local scales, which vanish in the averaging process. The experimental data and the corresponding simulations are therefore based on the pulse intensities $|u_n^m|^2$ of the shorter loop.

To evaluate the first- and second-order scattering processes, we derive the dispersion relation for the disorder-free system. For a uniform time-independent potential, $\varphi_u(n,m) = \varphi_0 \in \mathbb{R}$, we introduce the Floquet-Bloch Ansatz to deduce the dispersion relation $2\cos(\Theta) = \cos(Q) - 1$, with solutions of the form $u_n^m = U(Q, \Theta)e^{iQn/2}e^{-i\Theta m/2}$ and $v_n^m = V(Q, \Theta)e^{iQn/2}e^{-i\Theta m/2}$ (Fig. 3b). Each plane-wave solution is characterized by a Bloch momentum $Q \in [-\pi, \pi]$ and a propagation constant $\Theta \in [-\pi, \pi]$ (corresponding to k and β, respectively, in Eqs. 1 and 2). Typically, in this system, wavepackets in the vicinity of $Q = \pm\pi$ have the highest group velocity but the lowest group velocity dispersion, whereas wavepackets with the lowest momentum $Q \approx 0$ experience low group velocity but the highest dispersion.

Since we are interested here in studying the propagation of wavepackets in different spectral regions (corresponding to Fig. 2), we excite a spectrally narrow region by creating a spatially-broad Gaussian beam $u_n = \exp\left(-n^2/2n_w^2\right)\exp(-iQn/2)$, with $n_w = 30$, launched with central momentum of $Q = 0.8\pi$. The generation of the Gaussian beam relies on a non-Hermitian diffusion process[51], allowing to maintain an extremely stable phase relation between the optical pulses (see details in the last section of the SI[37]). The experimental results (Fig. 3d) show the sequential build-up of the Gaussian beam (time steps $m \leq 155$) and subsequently the desired free propagation (time steps $m > 155$) with $Q = 0.8\pi$ in the homogeneous system ($\varphi_u = 0$). The

propagation of this synthetically constructed Gaussian wavepacket shows the desired width and tilt (Fig. 3d). In the absence of any potential, this synthetic beam exhibits diffraction broadening, akin to propagation in homogeneous linear media.

To study the effects of disorder in our synthetic lattice, it is essential to explain the phase the pulses accumulate, φ_u, which is analogous to the phase accumulated by passing through a potential term in Schrödinger's equation. For example, a phase $\varphi_u(n,m) = \sin(Q_0 n)$ is equivalent to a periodic single-frequency (sinusoidal) potential that scatters a plane wave with wavenumber Q to a plane wave with $Q + Q_0$. As in any scattering process, here too, first-order transitions dominate the process, but in principle, two-step transition, e.g. $-Q_0 \rightarrow 0$ followed by a second transition $0 \rightarrow Q_0$, are also possible because the overall transition conserves the quasi-energy Θ (analogous to the longitudinal momentum in Eqs. 1,2). The efficiency of such second-order transitions is, here too, usually low because $Q = 0$ is a virtual level. This makes it clear why Anderson localization via these second-order transitions has thus far never been observed.

We now proceed to implement the bandwidth-limited disordered potential as described above (Fig. 1b) in our synthetic lattice. First, the potential has to be evolution-invariant; otherwise – if the potential varies throughout propagation – the beam will undergo diffusion or hyper-transport but not localization[20]. To do that, we choose a random potential $\varphi_u(n)$ that is constant with every time-step m, so as to make the disorder propagation-invariant. We generate the disorder to have the power spectrum $S_\varphi(Q) = |FT\{\varphi_u(n)\}|^2$ comprising many spectral components with random amplitude and phase, all restricted to a small region around some frequency Q_0. The spectrum of the disordered potential is nonzero only around $Q_0 = \pm 0.4\pi$ with width $\Delta Q_0 \simeq 0.2|Q_0|$ (similar to k_0 and Δk in Fig. 1b). Finally, we launch a broad Gaussian beam ($n_w = 50$) with a central momentum Q and launch it into the disordered synthetic lattice. Figure 4 presents the measured

ensemble average over 100 wave propagation experiments, each for a different realization of the disorder, but with the same not-zero range of $S_\varphi(Q)$ and same disorder strength, A_{DS}, defined by the norm of $S_\varphi(Q)$. We repeat this experiment for several initial momenta Q of the Gaussian beam, which is equivalent to several angles of incidence in the transverse localization scheme of Eq. (1).

Figure 4 shows the ensemble-averaged intensity as it evolves in the disordered synthetic lattice. We examine the trajectories of the ensemble-averaged beams, and search for the hallmark feature of Anderson localization: localized wavepackets that come to a halt irrespective of their initial momentum. We find that for certain Q-values, the beams maintain their initial trajectories and exhibit diffraction broadening, unaffected by localization processes, as if there is no disorder, whereas beams with other Q-values change their initial trajectories to propagate parallel to the time-step axis (zero transverse velocity), irrespective of their initial momentum, and stop expanding in their width (Fig. 4a). These latter Q values correspond to localization by first-order transitions at $Q = Q_0/2$ (more efficient transitions, narrower localized beam) and by second order transition at $Q = Q_0$ (less efficient, broader beam). In addition, we find that beams launched at Q=0 stop expanding, again due to second order localization, manifesting localization at low wavenumbers. The dominant process that causes this type of localization is a series of symmetric scatterings to virtual states and back, which naturally occurs in any Hermitian system, irrespective of its spectral shape. We find that this phenomenon of localization by strictly small-scale disorder (smaller than the wavelength) takes a larger distance to set in, hence the losses should be minimized for observing this new phenomenon in experiments. In addition, we also find localization at Q=0.25, which occurs by the process of bandwidth expansion due to strong disorder (see the discussion in the fourth section of the SI[37]). On the other hand, we find that at other Q values, e.g., $Q = 0.75Q_0$ and $1.2Q_0$, the beam has almost no interaction with the disordered

potential, and continues on its initial trajectory undergoing nearly free-diffraction, as if the underlying lattice were disorder-free.

Next, we extract the effective width for each initial momentum (Fig. 4b), after a large propagation time in the system. The effective width displays several local minima around initial momentum 0, $Q_0/2$ and Q_0, which serves as a direct indication for Anderson localization, and conforms with the respective theoretical plot in Fig. 2a (calculated for the transverse localization scheme of Eq. 1). Altogether, the zero transverse velocity and the arrest of diffraction-broadening for $Q = Q_0$ and Q=0, displayed in Fig. 4, are direct experimental evidence for localization outside the spectral extent of the disorder.

Finally, we study several additional features of localization by second-order transitions, by extracting the spatial intensity distribution (after large propagation times) from the experimental data and comparing to those of "ordinary" (first-order) localization. Figure 5 shows the characteristic exponential decay of the ensemble-average wavepackets, at $Q = 0$, at $Q_0/2$ and also at Q_0, respectively. For each initial Q, we use a suitable width for the initial wavepacket, in order to excite a minimal number of localized modes in each regime (i.e., a too wide initial beam might excite many narrow localized modes, so that the shape of the propagating wavepacket would remain similar to the input beam) As the disorder is made stronger, the localized wavefunctions become narrower and acquire an exponential shape, despite some asymmetry present due to their initial non-zero group velocity. This happens not only at $Q_0/2$ (first-order localization) but also at Q=0 and $Q = Q_0$, where localization is by strictly by second-order localization processes. At the strongest disorder all wavepackets are exponentially localized and are all centered around n=0 (zero transverse velocity), irrespective of their initial momentum. We extract the localization

length and find that in all cases it is at least an order of magnitude smaller than the system size, assuring that all the effects observed are not affected by the system size.

In conclusion, we presented the first experiments showing Anderson localization completely outside the spectral extent of the disorder, both at very low and at very high wavenumbers. The localization at low wavenumbers is especially intriguing: it implies that localization will always occur at low wavenumbers – even when the spectrum of the disorder is strictly at high wavenumbers. This feature is universal, arising from the symmetry of the power spectrum of the disorder, and it is therefore expected to occur for any Hermitian system. Overall, the phenomenon of localization by high-order scattering processes implies that even if a system is highly correlated (e.g., amorphous structures[22,51–53] or hyperuniform materials[54]), waves of any wavenumber, even those beyond the disorder spectrum, can experience Anderson localization. In this vein, it should be possible to observe short localization lengths induced strictly by third-order transitions or higher. We anticipate that new mobility edges would be induced by virtual transitions in 2D and 3D, and also in higher dimensions that include disorder in synthetic-space[55]. Our results expand the understanding of disordered systems, and suggest developing the notion of bandwidth-limited disorder for controlling the localization and transport in desired spectral ranges. It is interesting to witness that Anderson Localization, initiated more than 60 years ago, continues to generate new ideas and surprises, exemplifying one of the most fascinating phenomena in nature: the interaction between waves and disorder.

References

1. Titus Lucretius Carus. *De rerum natura ("On the nature of things"), circa 60BC.*

2. Drude, P. Zur Elektronentheorie der Metalle. *Ann. Phys.* **306**, 566–613 (1900).

3. Anderson, P. W. Absence of Diffusion in Certain Random Lattices. *Phys. Rev. Lett.* **109**, 1492 (1958).

4. Abdullaev, S. S. & Zaslavskii, G. M. Nonlinear dynamics of rays in inhomogeneous media. *Zhurnal Eksp. i Teor. Fiz.* **80**, 524–536 (1981).

5. Hodges, C. H. Confinement of vibration by structural irregularity. *J. Sound Vib.* **82**, 411–424 (1982).

6. John, S. Electromagnetic absorption in a disordered medium near a photon mobility edge. *Phys. Rev. Lett.* **53**, 2169 (1984).

7. Raedt, H. De, Lagendijk, A. & de Vries, P. Transverse Localization of Light. *Phys. Rev. Lett.* **62**, 2–5 (1989).

8. Wiersma, D. S., Bartolini, P., Lagendijk, A. & Righini, R. Localization of light in a disordered medium. *Nature* **390**, 671–673 (1997).

9. Berry, M. V. & Klein, S. Transparent mirros: rays, waves and localization. *Eur. J. Phys.* **18**, 222 (1997).

10. Störzer, M., Gross, P., Aegerter, C. M. & Maret, G. Observation of the Critical Regime Near Anderson Localization of Light. *Phys. Rev. Lett.* **96**, 063904 (2006).

11. Chabanov, A. A., Stoytchev, M. & Genack, A. Z. Statistical signatures of photon localization. *Nature* **404**, 850–853 (2000).

12. Kuhl, U., Izrailev, F. M., Krokhin, A. A. & Stöckmann, H. J. Experimental observation of the mobility edge in a waveguide with correlated disorder. *Appl. Phys. Lett.* **77**, 633–635

(2000).

13. Schwartz, T., Bartal, G., Fishman, S. & Segev, M. Transport and Anderson localization in disordered two-dimensional photonic lattices. *Nature* **446**, 52–55 (2007).

14. Lahini, Y. *et al.* Anderson Localization and Nonlinearity in One-Dimensional Disordered Photonic Lattices. *Phys. Rev. Lett.* **100**, 013906 (2008).

15. Karbasi, S. *et al.* Image transport through a disordered optical fibre mediated by transverse Anderson localization. *Nat. Commun.* **5**, 1–9 (2014).

16. Hu, H., Strybulevych, A., Page, J. H., Skipetrov, S. E. & van Tiggelen, B. A. Localization of ultrasound in a three-dimensional elastic network. *Nat. Phys.* **4**, 945–948 (2008).

17. Billy, J. *et al.* Direct observation of Anderson localization of matter waves in a controlled disorder. *Nature* **453**, 891–894 (2008).

18. Roati, G. *et al.* Anderson localization of a non-interacting Bose–Einstein condensate. *Nature* **453**, 895–898 (2008).

19. Barthelemy, P., Bertolotti, J. & Wiersma, D. S. A Lévy flight for light. *Nature* **453**, 495–498 (2008).

20. Levi, L., Krivolapov, Y., Fishman, S. & Segev, M. Hyper-transport of light and stochastic acceleration by evolving disorder. *Nat. Phys.* **8**, 912–917 (2012).

21. Sheinfux, H. H. *et al.* Observation of Anderson localization in disordered nanophotonic structures. *Science* **356**, 953–956 (2017).

22. Rechtsman, M. *et al.* Amorphous photonic lattices: Band gaps, effective mass, and suppressed transport. *Phys. Rev. Lett.* **106**, 193904 (2011).

23. Haberko, J., Froufe-Pérez, L. S. & Scheffold, F. Transition from light diffusion to localization in three-dimensional amorphous dielectric networks near the band edge. *Nat.*

Commun. **11**, 1–9 (2020).

24.   Wang, P. *et al.* Localization and delocalization of light in photonic moiré lattices. *Nature*
        557, 42–46 (2020).

25.   Tzortzakakis, A. F., Makris, K. G. & Economou, E. N. Non-Hermitian disorder in two-
        dimensional optical lattices. *Phys. Rev. B* **101**, 014202 (2020).

26.   Abrahams, E., Anderson, P. W., Licciardello, D. C. & Ramakrishnan, T. V. Scaling
        Theory of Localization: Absence of Quantum Diffusion in Two Dimensions. *Phys. Rev.*
        Lett. **42**, 673–676 (1979).

27.   Dunlap, D. H., Wu, H. L. & Phillips, P. W. Absence of localization in a random-dimer
        model. *Phys. Rev. Lett.* **65**, 88 (1990).

28.   Izrailev, F. M. & Krokhin, A. A. Localization and the mobility edge in one-dimensional
        potentials with correlated disorder. *Phys. Rev. Lett.* **82**, 4062 (1999).

29.   John, S. & Stephen, M. J. Wave propagation and localization in a long-range correlated
        random potential. *Phys. Rev. B* **28**, 6358 (1983).

30.   John, S. Strong localization of photons in certain disordered dielectric superlattices. *Phys.*
        Rev. Lett. **58**, 2486–2489 (1987).

31.   Lifshits, I. M., Gredeskul, S. A. & Pastur, L. A. *Introduction to the Theory of Disordered*
        Systems. (Wiley-VCH, 1988).

32.   Flores, J. C. Transport in models with correlated diagonal and off-diagonal disorder. *J.*
        Phys. Condens. Matter **1**, 8471 (1989).

33.   Gurevich, E. & Kenneth, O. Lyapunov exponent for the laser speckle potential : A weak
        disorder expansion. *Phys. Rev. A* **79**, 063617 (2009).

34.   Bellani, V. *et al.* Experimental evidence of delocalized states in random dimer

superlattices. *Phys. Rev. Lett.* **82**, 2159 (1999).

35. Lugan, P. *et al.* One-dimensional Anderson localization in certain correlated random potentials. *Phys. Rev. A* **80**, 023605 (2009).

36. Dikopoltsev, A., Herzig Sheinfux, H. & Segev, M. Localization by virtual transitions in correlated disorder. *Phys. Rev. B* **100**, 140202 (2019).

37. See supplementary materials.

38. Rechtsman, M. C. *et al.* Photonic Floquet Topological Insulators. *Nature* **496**, 196–200 (2012).

39. Plotnik, Y. *et al.* Experimental observation of optical bound states in the continuum. *Phys. Rev. Lett.* **107**, 28–31 (2011).

40. Stützer, S. *et al.* Photonic topological Anderson insulators. *Nature* **560**, 461–465 (2018).

41. Segev, M., Silberberg, Y. & Christodoulides, D. N. Anderson localization of light. *Nat. Photonics* **7**, 197–204 (2013).

42. Samelsohn, G., Gredeskul, S. A. & Mazar, R. Resonances and localization of classical waves in random systems with correlated disorder. *Phys. Rev. E* **60**, 6081 (1999).

43. Schreiber, A. *et al.* Photons walking the line: A quantum walk with adjustable coin operations. *Phys. Rev. Lett.* **104**, 050502 (2010).

44. Schreiber, A. *et al.* Decoherence and disorder in quantum walks: From ballistic spread to localization. *Phys. Rev. Lett.* **106**, 2011 (2011).

45. Regensburger, A. *et al.* Parity-time synthetic photonic lattices. *Nature* **488**, 167–171 (2012).

46. Wimmer, M., Miri, M. A., Christodoulides, D. & Peschel, U. Observation of Bloch oscillations in complex PT-symmetric photonic lattices. *Sci. Rep.* **5**, 1–8 (2015).

47.	Wimmer, M. *et al.* Observation of optical solitons in PT-symmetric lattices. *Nat. Commun.* **6**, 1–9 (2015).

48.	Muniz, A. L. M. *et al.* 2D Solitons in P T -Symmetric Photonic Lattices. *Phys. Rev. Lett.* **123**, 253903 (2019).

49.	Wimmer, M., Price, H. M., Carusotto, I. & Peschel, U. Experimental measurement of the Berry curvature from anomalous transport. *Nat. Phys.* **13**, 545–550 (2017).

50.	Weidemann, S. *et al.* Topological funneling of light. *Science* **368**, 311–314 (2020).

51.	Jin, C., Meng, X., Cheng, B., Li, Z. & Zhang, D. Photonic gap in amorphous photonic materials. *Phys. Rev. B* **63**, 195107 (2001).

52.	Mitchell, N. P., Nash, L. M., Hexner, D., Turner, A. M. & Irvine, W. T. M. Amorphous topological insulators constructed from random point sets. *Nat. Phys.* **14**, 380–385 (2018).

53.	Zhou, P. *et al.* Photonic amorphous topological insulator. *Light Sci. Appl.* **9**, 1–8 (2020).

54.	Leseur, O., Pierrat, R. & Carminati, R. High-density hyperuniform materials can be transparent. *Optica* **3**, 763 (2016).

55.	Lustig, E. *et al.* Experimentally Realizing Photonic Topological Edge States in 3D. in *Conference Proceedings - Lasers and Electro-Optics Society Annual Meeting-LEOS* (2020).
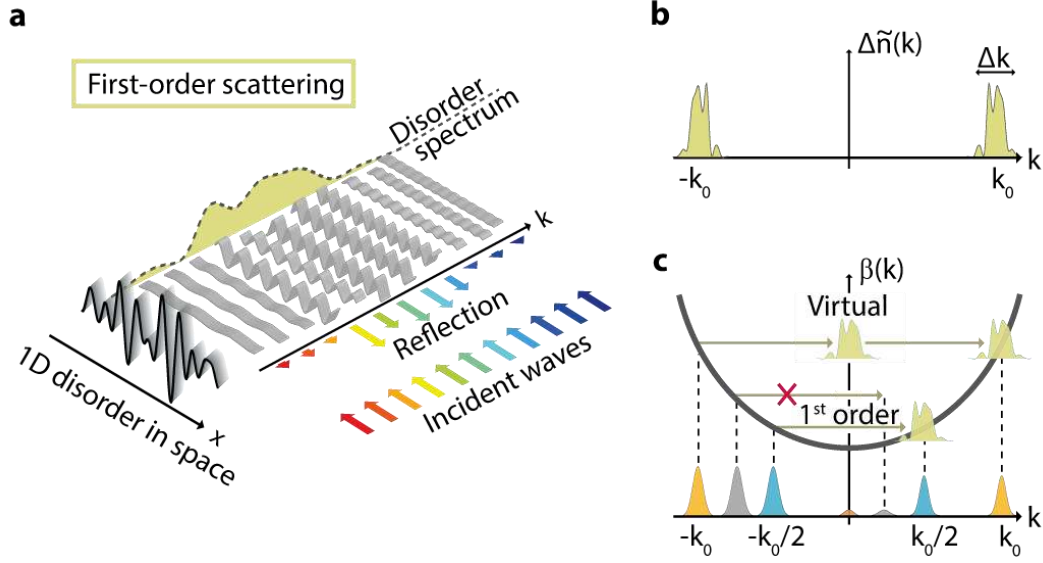
Fig. 1 | Localization through spectrally-dependent scattering and transitions. a, Localization via first-order scattering: waves with different wavenumbers k (different colors) undergo scattering events that depend on the spectral decomposition of the potential. **b,** The bandwidth-limited spectrum of correlated-disorder, $\Delta\tilde{n}(k)$, representing gratings with random amplitude and phase. The nonzero components lie in the intervals $[\pm k_0 - \Delta k, \pm k_0 + \Delta k]$. **c,** Scattering processes mediated by a single spectral component k_o (from $\Delta\tilde{n}(k)$), with the dispersion curve $\beta(k) = k^2/2\beta$ describing the phase-mismatch. A first-order phase-matched transition: a wave of wavenumber $-k_0/2$ scatters efficiently to $k_0/2$, because $\beta(-k_0/2) = \beta(k_0/2)$. A second-order phase-matched transition takes place when a wave scatters from $-k_0$ to 0 and subsequently to k_0. The intermediate state at $k = 0$ is called "virtual" because it is phase-mismatched with the initial wave $\beta(-k_0)$ unequal to $\beta(0)$. With the grating component at $\pm k_0$ there is no phase-matched scattering for a wave that starts with $-0.75k_0$.
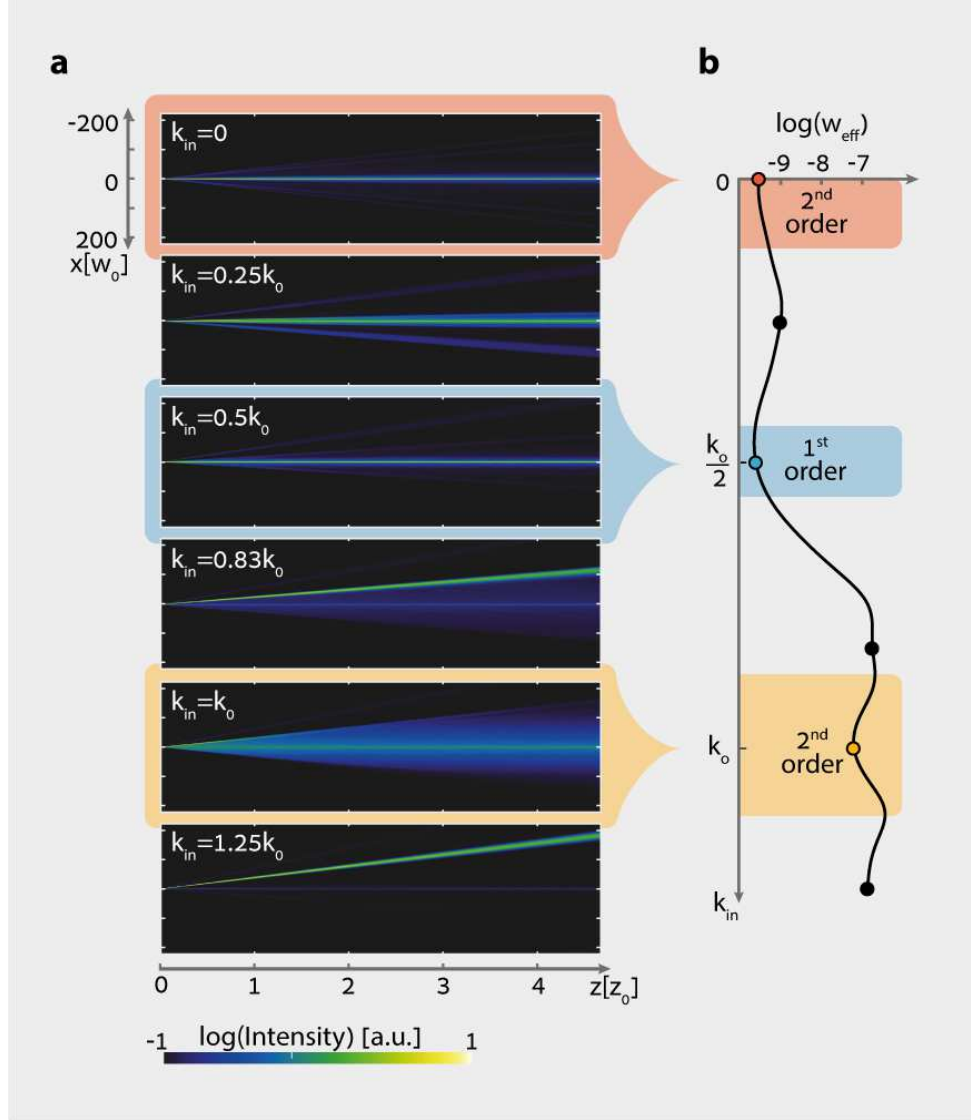
Fig 2. | Simulated first- and second-order localization under correlated disorder. a, Ensemble-averaged propagation in bandwidth-limited disorder, contained within a Δk region centered around $\pm k_0$. The input beam is a Gaussian wavepacket launched at chosen initial momenta corresponding to different wavenumber (k_{in}) values. At $k_{in} = 0$ the natural diffraction-broadening is arrested due to a second-order process. At $k_{in} = 0.25k_0$, the wavepacket is within the extended spectral extent of the strong correlated-disorder and therefore localizes. For $k_{in} = k_0/2$ localization occurs due to phase-matched first-order transitions. On the other hand, for $k_{in} = 0.83k_0$ and $k_{in} = 1.25k_0$, all transitions are phase-mismatched, so the wavepacket evolves almost unaffected by the disorder. When $k_{in} = k_0$, second-order processes induce localization. Initially, the wave packet expands but after some distance the expansion stops. We use normalized units for x and z (with the initial beam width w_0 and the Rayleigh length z_0, respectively). **b,** Effective width of wavepackets after propagation. The dip in the effective width indicating localization occurs in three regions: first-order localization (orange) and localization due to second order transitions (blue and green). Notice three local minima in the effective widths at $k_{in} = 0, k_0/2$ and k_0. (See Supp. Information for parameters).
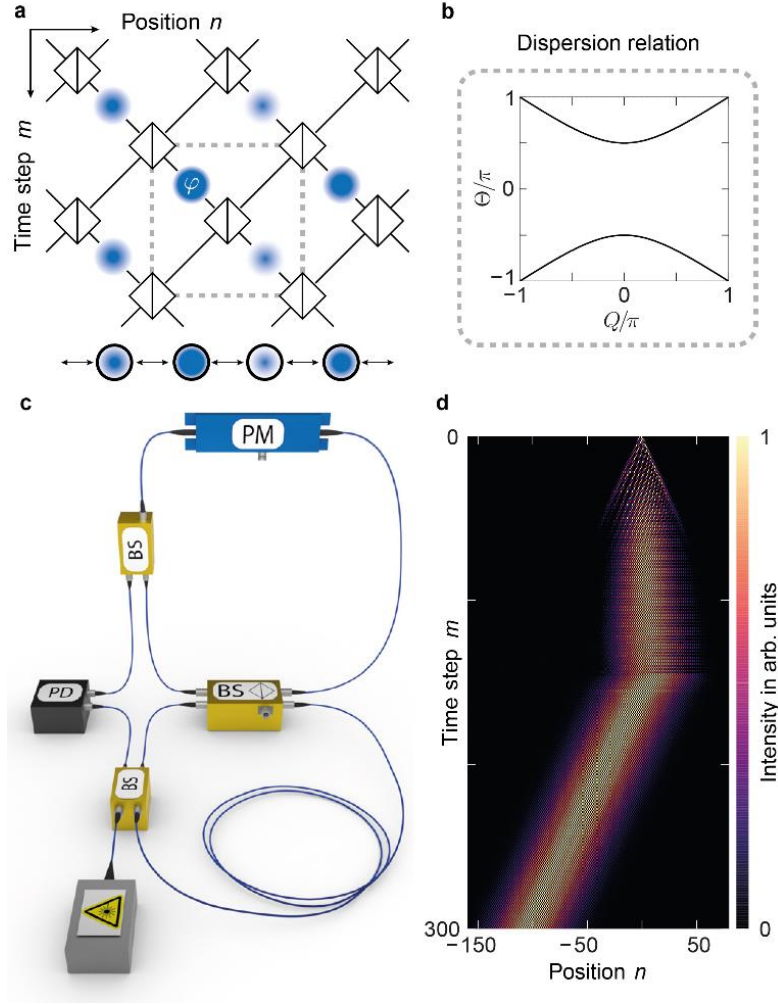
Fig. 3 | Synthetic photonic lattices and experimental setup. a, Double-discrete synthetic photonic lattice consisting of a mesh of beam-splitters, and its equivalent one-dimensional chain of sites. Phase modulation φ_u of spatially random distribution (blue circles with strength varying in n) corresponds to a disordered on-site potential of the chain. **b,** Dispersion relation of the disorder-free homogenous photonic lattice, where Q corresponds to the quasi-momentum and Θ to the quasi-energy (propagation constant), respectively. **c,** Experimental setup (simplified) consisting of two optical fiber loops, one shorter than the other, coupled by a beam splitter (BS). A laser pulse is injected into the loops. The pulse propagation in the loops can be mapped onto a 1+1 dimensional double-discrete lattice shown in **a**. The pulse intensities are measured with a photodetector (PD). A phase modulator (PM) shapes the real part of the lattice potential. **d,** Experimental data showing the creation of a Gaussian wavepacket to excite $Q = 0.8\pi$ in the upper band of the dispersion relation. Starting from a single pulse, a discrete diffraction pattern is formed, and manipulated to reach a Gaussian shape with a defined momentum (time steps $m = 1 \ldots 155$). From $m = 156$, the Gaussian beam of width $n_w = 30$ with a mean momentum of $Q = 0.8\pi$ propagates in the homogenous (disorder-free) Hermitian lattice.
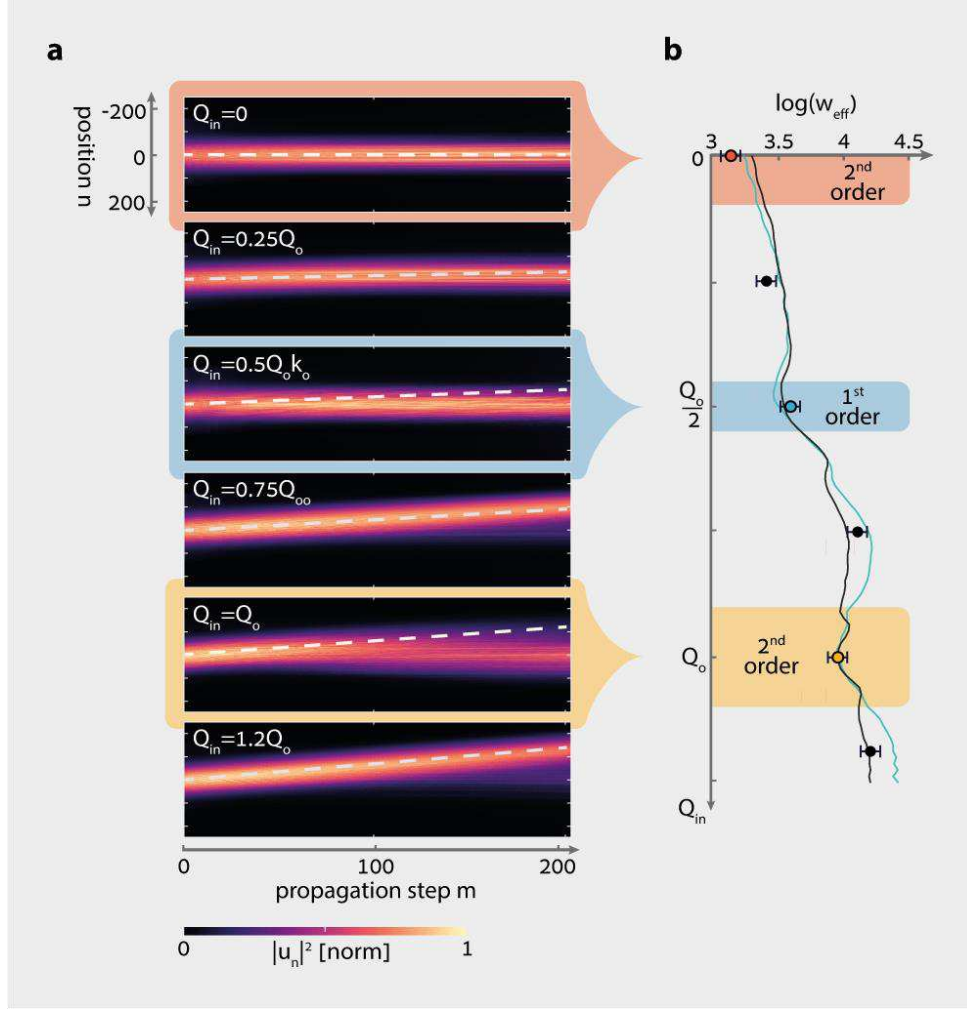
Fig 4. | Experimental observation of localization outside the spectral extent of the disorder.
a, Experimentally measured ensemble-averaged propagation of an initially Gaussian wavepacket launched at various initial momenta Q_{in}. The white lines mark the beam trajectory in the absence of disorder. At $Q_{in} = 0$ the wavepacket evolves without expanding due to second-order processes (as opposed to the natural diffraction-broadening in a homogenous potential). At $Q_{in} = 0.25Q_o$ the wavepacket is within the spectral extent of the disorder and therefore localizes. For $Q_{in} = 0.5Q_0$, multiple first-order transitions are phase-matched, hence the wavepacket localizes: it evolves to on-axis propagation and stops expanding. For $Q_{in} = 0.75Q_o$, the transitions are energy-mismatched, so the wavepacket continues on its initial trajectory and expands, as if it was unaffected by the disorder. At $Q_{in} = Q_o$, we find evolution in the regime of strictly second-order localization processes. Initially, the wavepacket expands but after some distance the expansion stops and the beam propagates on-axis. For $Q_{in} = 1.2Q_o$, the transitions are again phase-mismatched, so the wavepacket is unaffected by the disorder. **b,** Effective width vs initial quasi-momentum Q at the end of the propagation, showing local minima exactly in the first-order and second-order localization regions. The measured values (circles with error bars) qualitatively agree with the theoretical calculation (black). The blue curve displays simulated results for a larger lattice (beyond reach of our experiments), underlining the main trends found in the experiments.
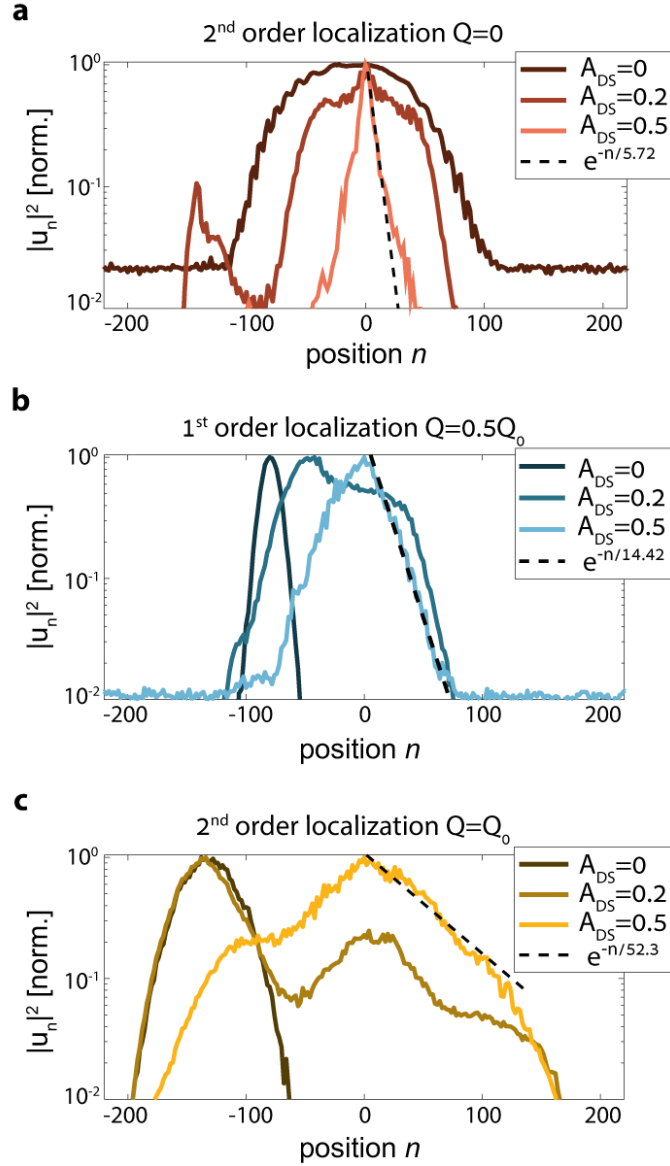
Fig 5. | Experimental signatures of Anderson localization inside and outside the spectral extent of the disorder. **a**-**c**, Shape of the ensemble-averaged beam after propagation in the synthetic photonic lattice with bandwidth-limited disorder, each for three different values of disorder strength, A_{DS}, ranging from zero to strong disorder. The initial widths of the wavepackets for $Q = 0, 0.5Q_0, Q_0$ are $n_w = 3.5, 10, 30$, respectively. As the disorder is made stronger, the wavefunctions become localized and exhibit exponential decay. This happens not only at $Q = 0.5Q_0$ by first-order processes (**b**) but also at $Q = 0$ (**a**) and at $Q = Q_0$ (**c**), where localization stems strictly from second-order processes. For strong disorder, all wavepackets are exponentially localized and are centered around the initial site $n = 0$, irrespective of their initial momentum. We extract the localization length in all cases and find it to be at least an order of magnitude smaller than the system size ($n = -200 \ldots 200$). The slightly different baselines stem from different optical noise levels in the different experimental runs.

Methods
Experimental implementation

In this section, we briefly describe the experimental setup. The setup consists of two optical fiber loops, coupled by a beamsplitter as shown in Fig. 3c. For technical reasons, in each fiber loop additional optical components are incorporated. Each loop contains a spool of a single mode fiber (Corning® Vascade® LEAF® EP) to extend the round-trip time to approximately 30μs. By adding a standard single mode fiber patch cord into the u-loop, we create a difference in the roundtrip time between the loops of approximately 100ns. We use an optical fiber coupler (AC Photonics) to couple the photodetector (1.2 GHz InGaAs) and the seed pulse injection (see Fig. 3c). The seed pulse generation is based on a continuous wave DFB laser diode (JDS Uniphase, 2MHz linewidth, 1550nm center), where a rectangular 40-60ns pulse is cut out via intensity modulation. The intensity modulation relies on a Mach-Zehnder intensity modulator (SDL Integrated Optics Limited) and an acousto-optical modulator (Brimrose Corp.). To maintain a high signal-to-noise ratio, we employ erbium-doped fiber amplifiers (Thorlabs), which are optically gain-clamped by a continuous wave DFB laser diode at 1538nm. This pilot laser is inserted into the amplifier via wavelength division multiplexing couplers (AC Photonics) and afterwards removed with an optical bandpass filter (WL Photonics). To incorporate gain and loss for the preparation of the synthetic Gaussian beam, we place an acousto-optical intensity modulator in each loop. The output of the modulators is aligned to the 0th diffraction order, to avoid frequency shifts. The working point of the modulators is set to a value between 0 and 1. The amplifiers compensate the overall roundtrip losses in this setting. By varying the transmission of the intensity modulator, one can effectively achieve gain or loss. The beamsplitter connecting the fiber loops is a variable fiber optical coupler (Agiltron Inc.) that can electronically control the coupling between the two loops. We use a phase modulator (iXBlue Phot.) to control the phase of the pulses, and therefore the real part of the analogue lattice potential. In addition, we use a polarization controller (Thorlabs) for aligning the correct polarization for the LiNbO3-based components. The waveforms of the modulators are prepared with MATLAB and generated with arbitrary waveform generators (Keysight Tech.). For the data acquisition, the output voltages of the photo detectors are amplified (FEMTO HLVA-100) and then sampled with an oscilloscope (Rohde & Schwarz). The basis time scales T and Δt, which are required for mapping the pulse intensities on the 1+1 dimensional lattice, are extracted from a control experiment in a homogenous lattice with a single-site excitation. Finally, we apply a base-line correction to the experimental data, which filters out the optical noise floor.

Acknowledgements

Author Contributions

AD, SW and MK are equal-contribution first-authors. All authors contributed significantly to this work.

Competing Interest Declaration

The authors declare no competing interests.

Additional Information

Supplementary Information is available for this paper. The Supplementary Information contains explanations on the equivalence between the paraxial wave equation and the Schrodinger equation, the method we used to design the disorder in the spectral domain, the effect of increased spectral extent in strong and correlated disorder, effective width calculation in disordered systems, the implementation of the time-bin encoded photonic lattice we use as an experimental platform and the method we use to create a Gaussian beam in such a lattice.

Correspondence and requests for materials should be addressed to msegev@technion.ac.il
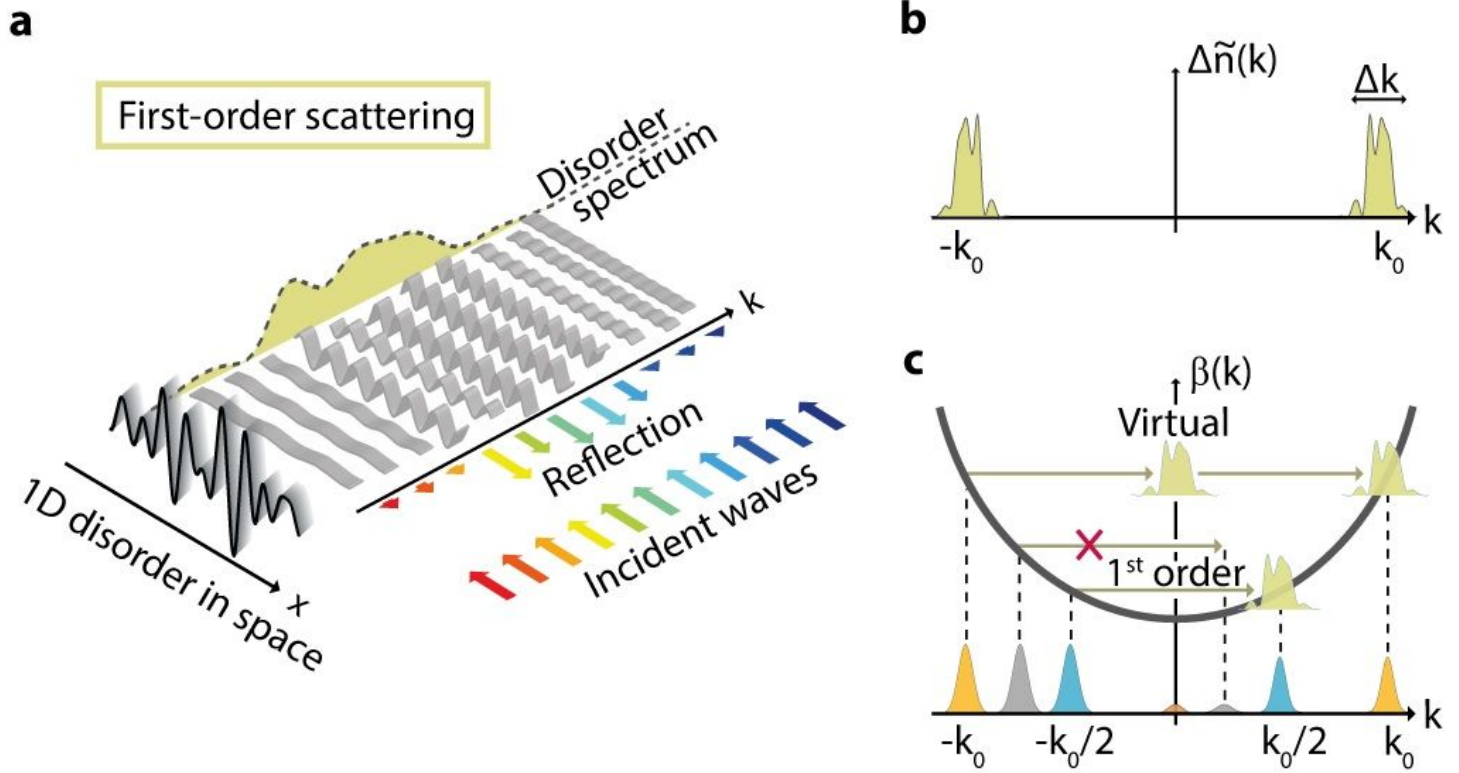
Figures

Figure 1

Localization through spectrally-dependent scattering and transitions. (see Manuscript file for full figure legend)
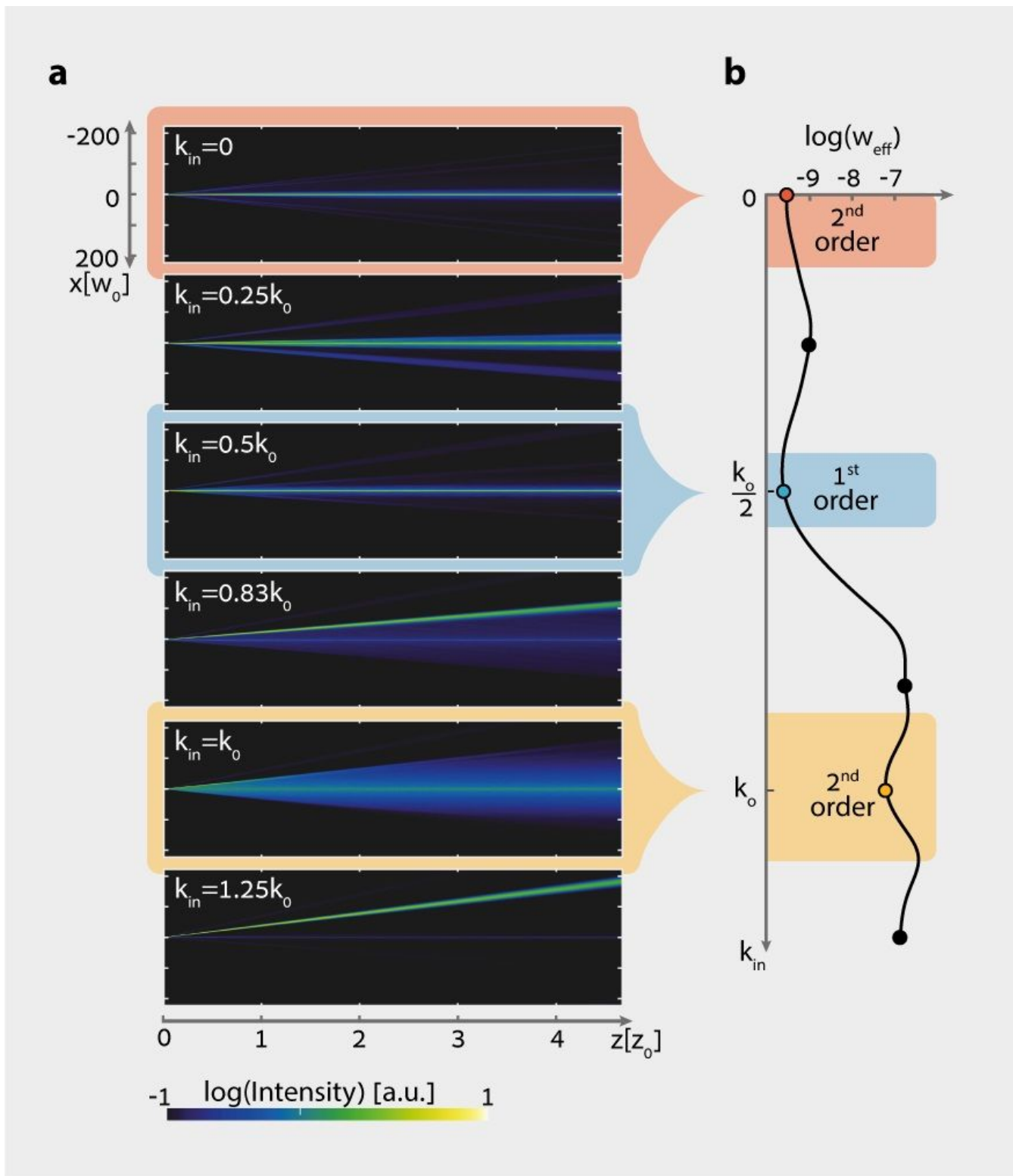
Figure 2

Simulated first- and second-order localization under correlated disorder. (see Manuscript file for full figure legend)
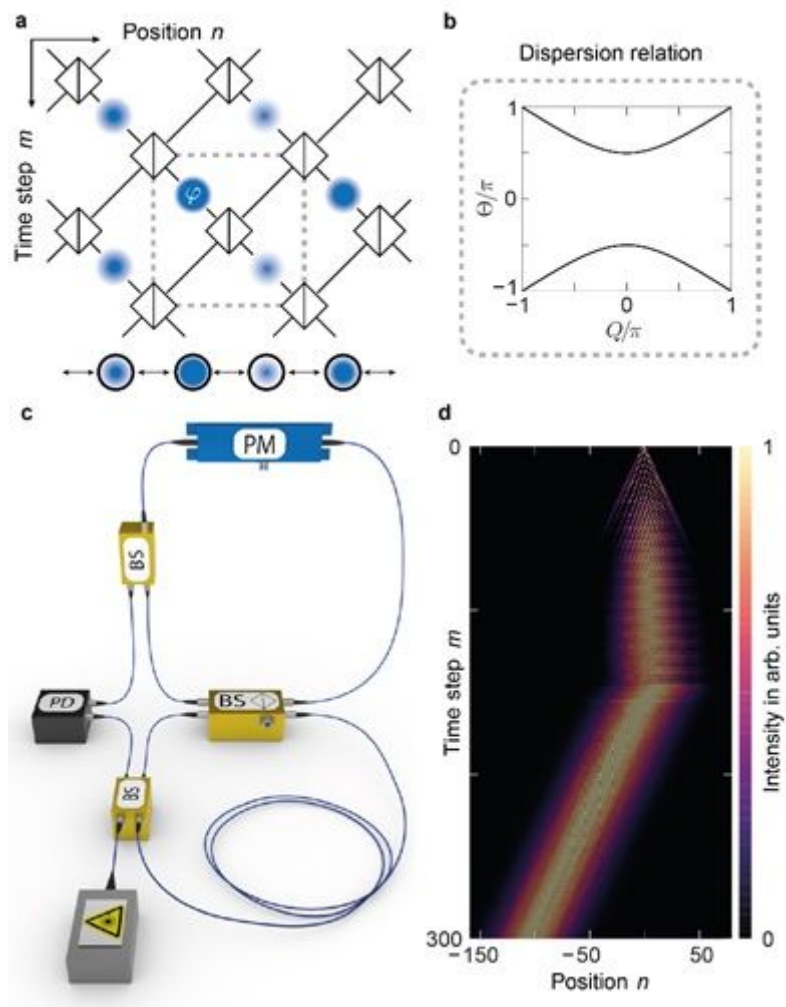
Figure 3

Synthetic photonic lattices and experimental setup. (see Manuscript file for full figure legend)
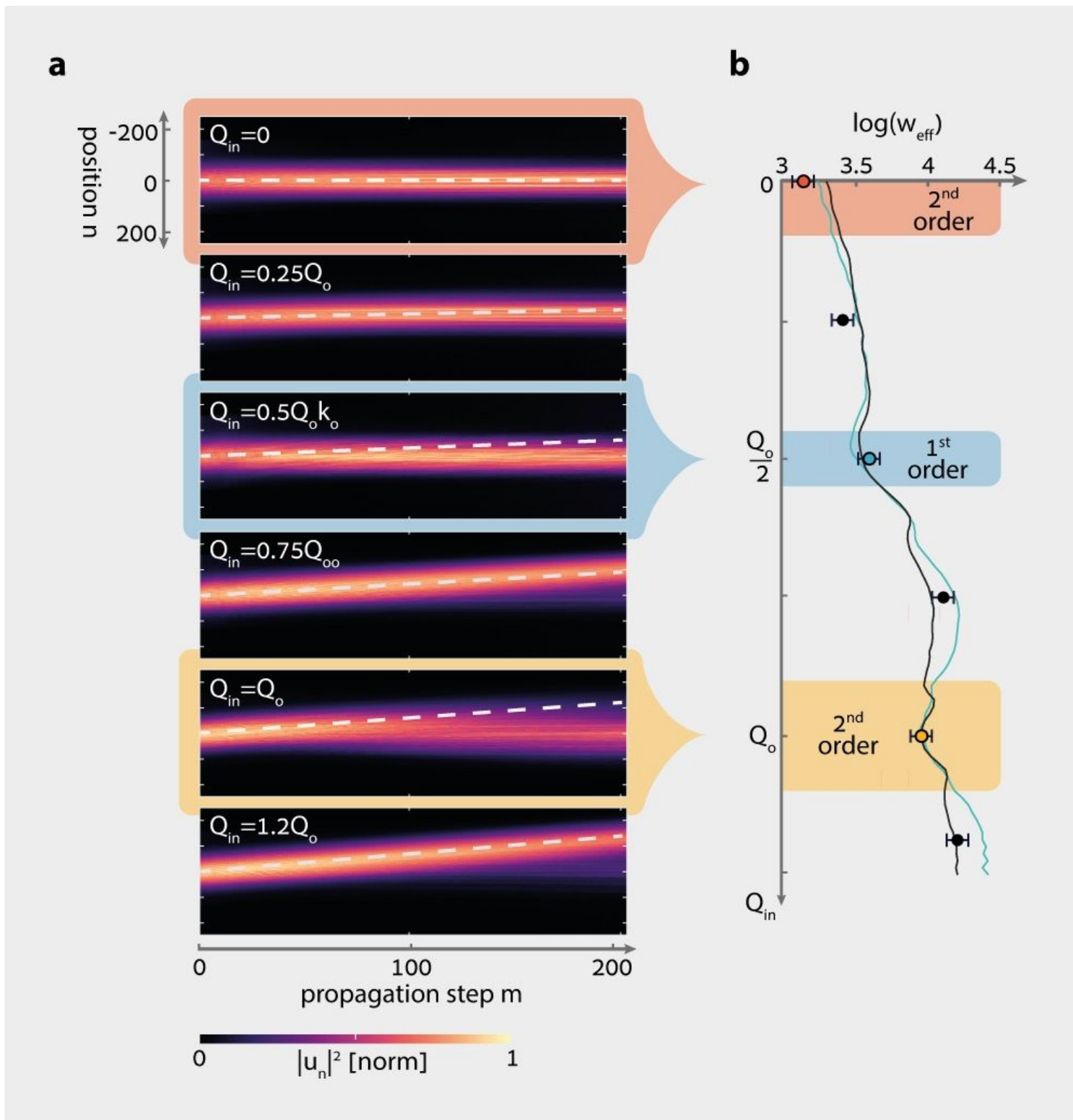
Figure 4

Experimental observation of localization outside the spectral extent of the disorder. (see Manuscript file for full figure legend)
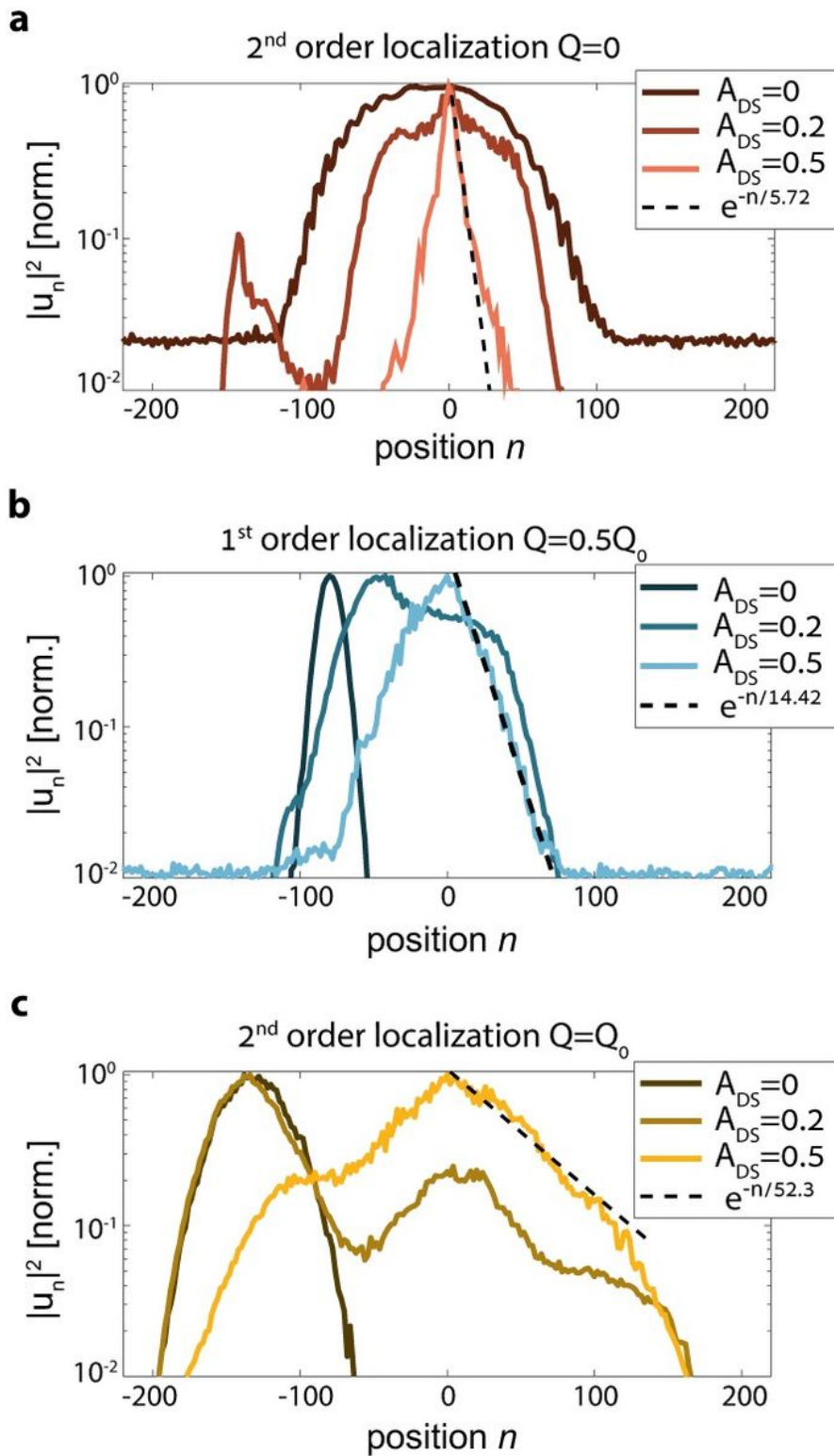
a

b

c

Figure 5

Experimental signatures of Anderson localization inside and outside the spectral extent of the disorder. (see Manuscript file for full figure legend)

Supplementary Files

This is a list of supplementary files associated with this preprint. Click to download.

- ExpALVTSIsubmitted.docx